

1 **Open Targets Genetics: An open approach to systematically prioritize causal variants**  
2 **and genes at all published GWAS trait-associated loci**

3  
4 Edward Mountjoy<sup>1,2</sup>, Ellen M. Schmidt<sup>1,2</sup>, Miguel Carmona<sup>2,3</sup>, Gareth Peat<sup>2,3</sup>, Alfredo Miranda<sup>2,3</sup>,  
5 Luca Fumis<sup>2,3</sup>, James Hayhurst<sup>2,3</sup>, Annalisa Buniello<sup>2,3</sup>, Jeremy Schwartzentruber<sup>1,2,3</sup>, Mohd  
6 Anisul Karim<sup>1,2</sup>, Daniel Wright<sup>1,2</sup>, Andrew Hercules<sup>2,3</sup>, Eliseo Papa<sup>4</sup>, Eric Fauman<sup>5</sup>, Jeffrey C.  
7 Barrett<sup>1,2</sup>, John A. Todd<sup>6</sup>, David Ochoa<sup>2,3</sup>, Ian Dunham<sup>1,2,3</sup>, Maya Ghousaini<sup>1,2,\*</sup>.

- 8  
9 1. Wellcome Sanger Institute, Wellcome Genome Campus, Hinxton, Cambridgeshire CB10  
10 1SA, UK  
11 2. Open Targets, Wellcome Genome Campus, Hinxton, Cambridgeshire CB10 1SD, UK  
12 3. European Molecular Biology Laboratory, European Bioinformatics Institute (EMBL-EBI),  
13 Wellcome Genome Campus, Hinxton, Cambridgeshire CB10 1SD, UK  
14 4. Systems Biology, Biogen, Cambridge, MA, 02142, United States  
15 5. Integrative Biology, Internal Medicine Research Unit, Pfizer Worldwide Research,  
16 Development and Medical, Cambridge, MA 02139, United States  
17 6. Wellcome Centre for Human Genetics, Nuffield Department of Medicine, NIHR Oxford  
18 Biomedical Research Centre, University of Oxford, Roosevelt Drive, Oxford, OX3 7BN,  
19 UK  
20 \* Corresponding author

21  
22  
23  
24

## 25 Abstract

26 Genome-wide association studies (GWAS) have identified many variants robustly associated  
27 with complex traits but identifying the gene(s) mediating such associations is a major challenge.  
28 Here we present an open resource that provides systematic fine-mapping and protein-coding  
29 gene prioritization across 133,441 published GWAS loci. We integrate diverse data sources,  
30 including genetics (from GWAS Catalog and UK Biobank) as well as transcriptomic, proteomic  
31 and epigenomic data across many tissues and cell types. We also provide systematic disease-  
32 disease and disease-molecular trait colocalization results across 92 cell types and tissues and  
33 identify 729 loci fine-mapped to a single coding causal variant and colocalized with a single  
34 gene. We trained a machine learning model using the fine mapped genetics and functional  
35 genomics data using 445 gold standard curated GWAS loci to distinguish causal genes from  
36 background genes at the same loci, outperforming a naive distance based model. Genes  
37 prioritized by our model are enriched for known approved drug targets (OR = 8.1, 95% CI: [5.7,  
38 11.5]). These results will be regularly updated and are publicly available through a web portal,  
39 Open Targets Genetics (OTG, <http://genetics.opentargets.org>), enabling users to easily  
40 prioritize genes at disease-associated loci and assess their potential as drug targets.

## 41 Introduction

42 Over 90% of GWAS-associated SNPs fall in non-coding regions, indicating that they affect  
43 expression of neighbouring genes through regulatory mechanisms<sup>1,2</sup>, which can act over long  
44 distances and affect more than one gene. Hence, identification of the causal gene(s) and cell or  
45 tissue site of action is a major challenge requiring detailed low-throughput analysis of individual  
46 loci. One default approach has been to assign the top trait-associated SNP to the closest gene  
47 at each locus. However relying on physical proximity alone can be misleading since SNPs can  
48 influence gene expression over long genomic ranges<sup>3</sup>, with studies based on eQTL data  
49 suggesting that two thirds of the causal genes at GWAS loci are not the closest<sup>4,5</sup>. To add to  
50 the challenge, associated SNPs often span large regions due to linkage disequilibrium (LD), and  
51 pinning down the functional SNP and the tissue or cell type which mediates its effect can be  
52 complicated.

53  
54 Connecting causal variants with their likely causal gene is a laborious process which requires  
55 the integration of GWAS data with multi-omics datasets across a wide range of cell types and

56 tissues such as expression and protein quantitative traits (eQTL and pQTL), chromatin  
57 accessibility and chromatin interaction datasets. Subsequent functional assessment (such as  
58 reporter assays and CRISPR/Cas9 genome editing) can then be used to confirm the  
59 relationship between a putative causal variant and the gene it regulates. Using these integrative  
60 approaches, systematic international efforts have been undertaken to translate GWAS  
61 associated signals into target genes focused on one or a small subset of phenotypes <sup>6-9</sup>.  
62 However, there are currently no resources that systematically prioritize all genes beyond  
63 specific therapy areas <sup>9</sup>. Therefore, there is a need for a comprehensive, unbiased, scalable and  
64 reproducible approach that leverages all the publicly available data and knowledge to assign  
65 genes systematically to published loci across the entire range of phenotypes and diseases.

66  
67 Drug development is hindered by a high attrition rate, with over 90% of the drugs that enter  
68 clinical trials failing, primarily due to lack of efficacy found in later, more costly stages of  
69 development <sup>10</sup>. Retrospective analyses have estimated that drugs are twice as likely to be  
70 approved for clinical use if their target is supported by underlying GWAS evidence <sup>11</sup>. Hence  
71 there is a critical need to build strategies that incorporate novel genetic discoveries and  
72 mechanistic evidence from GWAS and post-GWAS studies to suggest novel therapeutic targets  
73 for which to develop medicines, and ultimately increase the success rate of drug development.

74  
75 Here, we describe a universal solution to these challenges: a systematic and comprehensive  
76 analysis pipeline for integrating GWAS results with functional genomics data to prioritize the  
77 causal gene(s) at each published GWAS-associated locus. The pipeline performs fine-mapping  
78 and systematic disease-disease and disease-molecular trait colocalization analysis. We  
79 integrate information from GWAS, expression and protein quantitative trait loci (eQTL and  
80 pQTL) and epigenomics data (e.g. promoter capture Hi-C, DNase hypersensitivity sites). For  
81 gene prioritization we developed a machine learning model trained on a set of 445 curated gold-  
82 standard GWAS loci for which we have moderate or strong confidence in the functionally  
83 implicated gene. The model integrates the fine-mapping with the functional genomics data, gene  
84 distance, and in silico functional predictions to link each locus to its target gene(s). This output  
85 of this pipeline feeds into Open Targets Genetics (<https://genetics.opentargets.org>), a user-  
86 friendly, freely available, integrative web portal enabling users to easily prioritize likely causal  
87 variants and target genes at all loci and assess their potential as pharmaceutical targets through  
88 linking out to Open Targets Platform <sup>12,13</sup> and will be regularly updated as new data become  
89 available.

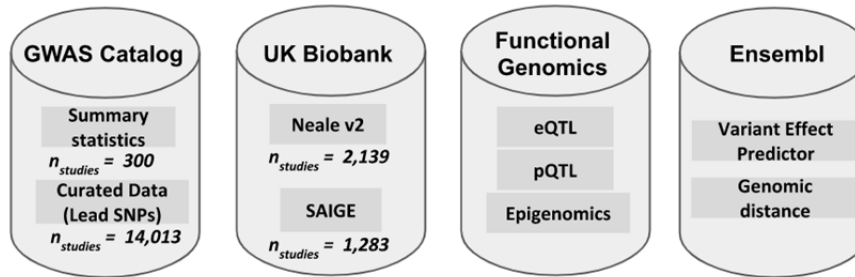
## 90 Results

### 91 Pipeline Overview

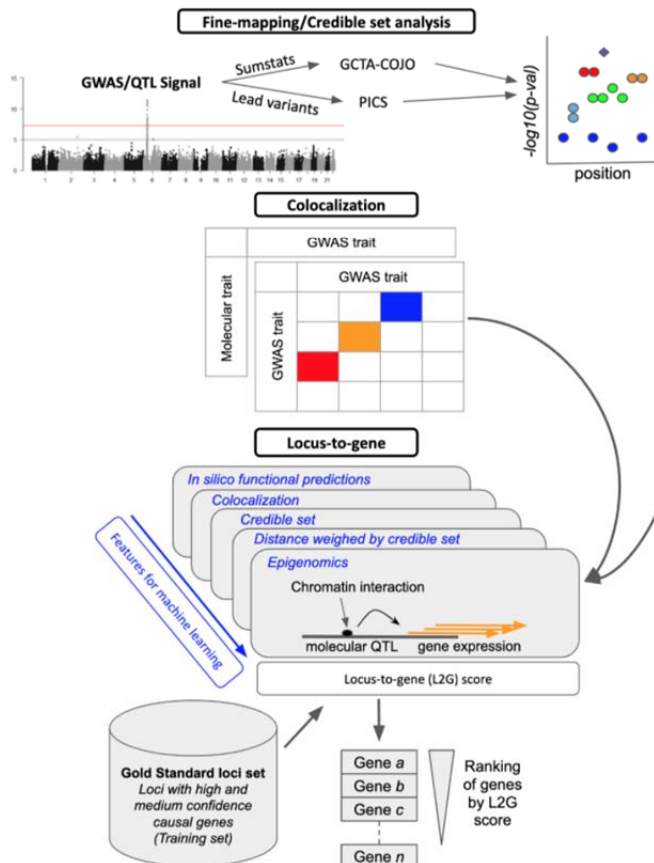
92 We harmonised and processed GWAS data from the GWAS Catalog and from UK Biobank, and  
93 conducted systematic fine mapping to generate sets of credibly causal variants across all  
94 133,441 study-lead variant associated loci. We also conducted cross-trait colocalization  
95 analyses for 3,621 GWAS studies with summary statistics available, which enabled us to  
96 identify traits and diseases that share common genetic etiology and mechanisms. To investigate  
97 whether changes in gene expression and protein abundance influence trait variation and  
98 disease susceptibility, we integrated 92 tissue- and cell type-specific molecular QTL datasets  
99 including GTEx <sup>14</sup>, eQTLGen <sup>15</sup>, the eQTL Catalogue <sup>16</sup> and pQTLs <sup>17</sup> and conducted  
100 systematic disease-molecular trait colocalization tests. Finally, we used a machine learning  
101 framework based on fine mapping, colocalization, functional genomics data and distance to  
102 prioritize likely causal genes at all trait-associated loci (Figure 1).

103

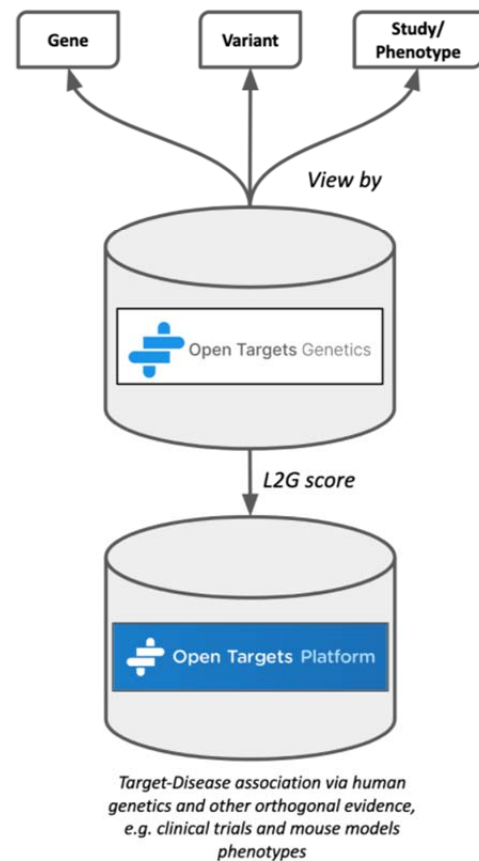
## a) DATA SOURCES & RESOURCES



## b) PIPELINES



## c) OUTPUT DATASETS



104

105 **Figure 1:** Open Targets Genetics pipeline schematic. a) Data sources include all available  
 106 GWAS, as well as variant effect predictions and functional genomic data. b) A number of  
 107 pipelines are run to perform statistical fine-mapping of GWAS, colocalization with gene  
 108 expression quantitative trait studies (QTLs) and also between distinct GWAS traits, and  
 109 integrative "locus-to-gene" prioritization from both genetic and functional genomic input features.  
 110 c) Outputs of the pipelines are available in a web portal, via programmatic API, and as bulk  
 111 downloads.

## 112 Fine mapping of all published genome-wide association studies

113 To establish a comprehensive resource linking variants and traits or diseases, we integrate  
114 GWAS studies both with and without full summary statistics. Full summary statistics were  
115 obtained from three sources: the NHGRI-EBI GWAS Catalog summary statistics database  
116 (number of studies ( $n_{\text{study}}$ ) = 300)<sup>18</sup>; binary phenotypes from UK Biobank as published by Zhou  
117 et al. ( $n_{\text{study}}$  = 1,283)<sup>19</sup> and all other UK Biobank phenotypes from the Neale lab ( $n_{\text{study}}$  = 2,139;  
118 downloaded 21/01/2019)<sup>20</sup> Studies with full summary statistics were restricted to those of  
119 predominantly European ancestries due to the lack of suitable reference genotypes required for  
120 conditional analysis from other populations. Studies without full summary statistics included all  
121 others in the NHGRI-EBI GWAS Catalog ( $n_{\text{study}}$  = 14,013)<sup>18</sup>. To prioritize candidate causal  
122 variants at each GWAS association, we performed fine mapping of 10,494 GWAS Catalog and  
123 UK Biobank studies. Two fine-mapping methods were used to maximise coverage of GWAS  
124 studies, one using full summary statistics and a second using linkage disequilibrium (LD)  
125 information only (see methods). For studies with full summary statistics, we first identified  
126 independent signals using GCTA-COJO<sup>21</sup> and then conducted per-signal conditional analysis  
127 adjusting for other independent signals in a region  $\pm 2$  Mb from the sentinel variant. We then  
128 used the Approximate Bayes Factor approach<sup>22</sup> to fine-map each conditionally independent  
129 signal. For studies without summary statistics, we used the PICS method<sup>23</sup> with an LD  
130 reference from the most closely matched 1000 Genomes superpopulation to estimate the  
131 probability that each variant is causal. Both methods output a posterior probability (PP) for each  
132 variant to be causal for the given association.

133  
134 A total of 133,441 sentinel variants were detected, with 53% of these being shared by more than  
135 one study (70,860 distinct sentinel variants). To assess the concordance of the two methods we  
136 compared the 95% credible sets after applying both methods to all loci from studies with  
137 summary statistics available. We found a median absolute difference in credible set size of 7  
138 variants (Supplementary Figure 1a), whereas the median credible set contained 17 variants. On  
139 average across loci, 70% of the credible set posterior probability collocated to the same variants  
140 between the two methods (Supplementary Figure 1b). These results suggest that on average  
141 the methods produced have comparable results. For subsequent analyses, we therefore used  
142 the full summary statistics method where these data were available, and for studies without  
143 summary statistics we used the PICS method.

144

145 Out of 133,441 loci association signals, 12,500 (9%) could be resolved to a single variant having  
146 PP > 0.95 and a further 21,279 (16%) to between 2 and 5 likely causal variants. Single-variant  
147 credible sets were 8.5 times more likely to have a moderate or high impact on protein-coding  
148 transcripts as predicted by the Ensembl variant effect predictor (VEP) <sup>24</sup> compared to variants in  
149 credible sets with 2 or more variants (OR=8.51,  $p < 2.2e^{-16}$ , Fisher's exact test). Outside coding  
150 regions, single-variant credible set variants were preferentially located in Ensembl Regulatory  
151 Build regulatory elements, including: promoters (OR=1.70,  $p < 2.2e^{-16}$ ), enhancers (OR=1.09,  
152  $p = 4.08e^{-4}$ ), transcription factor binding motifs (OR=1.85,  $p = 1.22e^{-15}$ ) or other open chromatin  
153 regions (OR=1.19,  $p = 4.8e^{-5}$ ).

154  
155 In order to identify GWAS signals with high-confidence evidence linking the trait to variant and  
156 variant to gene, we took single-variant resolution loci and filtered these to retain variants with  
157 moderate or high-impact coding consequences in VEP . We identified 2,284 single coding  
158 variants linking 378 genes to 303 traits (Supplementary Table 1). Among these were several  
159 known disease-causal gene associations and targets of approved therapies ( Supplementary  
160 Table 2) as well as novel disease-causal gene associations that had no prior evidence in the  
161 Open Targets Platform. One example is rs35383942, associated with breast cancer <sup>19,25</sup>, which  
162 is a predicted deleterious missense variant (Arg28Gln, CADD=24.3) in *PHLDA3* (Pleckstrin  
163 Homology Like Domain Family A Member 3). PHLDA3 is the direct target of TP53 and acts as a  
164 tumor suppressor gene through inhibition of AKT1, an oncogene that plays a pivotal role in cell  
165 proliferation and survival <sup>26</sup>.

## 166 Colocalization of GWAS and molecular traits

167 Since most associated variants are non-coding, it is expected that they influence disease risk  
168 through alteration in gene expression or splicing. One way to identify the target gene is to  
169 demonstrate that the statistical association of a GWAS locus and a gene expression QTL are  
170 colocalized -- that is, that the pattern of SNP associations is consistent with them sharing the  
171 same causal variant. We conducted systematic colocalization analysis <sup>27</sup> of GWAS loci with  
172 molecular trait QTLs from 92 tissues or cell types. The QTL datasets (Supplementary Table 3)  
173 include pQTLs for 2,994 plasma proteins assessed in 3,301 individuals of European descent <sup>17</sup>,  
174 eQTLs from 48 GTEx tissues (v7.0), blood eQTLGen <sup>15</sup>, and 14 eQTL studies from the newly  
175 established eQTL Catalogue, a resource of uniformly processed gene expression and splicing

176 QTLs recomputed from previously published datasets <sup>16</sup>. The results of the colocalization test  
177 are summarised by the probability, referred to as “H4”, that a causal variant is shared.

178  
179 GWAS-molecular QTL loci were tested if there was at least 1 variant overlapping in their 95%  
180 credible sets, suggesting prior evidence for colocalization (refer to methods). Of the 70,364 trait-  
181 associated loci from studies with summary statistics available, 49.4% had no colocalizing gene  
182 at an H4 threshold >0.8, 25.5% had exactly 1 colocalizing gene and 25.2% had >1 colocalizing  
183 gene. For loci with evidence of colocalization between GWAS and molecular QTL traits, 29%  
184 were specific to a single tissue or cell type, whereas 71% were observed across multiple  
185 tissues. We also examined non-coding QTLs that were fine-mapped to a single-variant  
186 resolution, and which colocalized with binary traits GWAS (H4>0.95). Results from this analysis  
187 are summarised in Supplementary Table 4.

188  
189 We also performed cross-trait colocalization across 3,621 GWAS to identify traits that are likely  
190 to be underpinned by the same molecular mechanism. A summary of the binary trait GWAS loci  
191 with the highest colocalization score (H4>0.95) is displayed in Supplementary Table 5. One  
192 example is a locus on chromosome 6 which colocalizes with asthma (6\_90220794\_T\_C) and  
193 Crohn’s disease (6\_90263440\_C\_A) suggesting that the two diseases may share common  
194 genetic etiology at this locus.

195  
196 To demonstrate the value of colocalization evidence, we examined coding variants that were  
197 fine-mapped to single-variant resolution, and which colocalized with a molecular QTL for the  
198 same gene (729 variants, Supplementary Table 6). Such cis-variants make good genetic  
199 instruments for testing the causal effect of the molecular phenotype on disease <sup>28</sup>, and the ratio  
200 of coefficients for the cis-variants is an estimate of the effect size of the molecular phenotype on  
201 disease. Using this approach we identified several known gene-trait associations. For example,  
202 missense variant rs34324219 is causal of changes in *TCN1* RNA and protein expression in  
203 whole blood <sup>15,17</sup> and also colocalizes (H4>0.99) with pernicious anemia, a disorder in which too  
204 few red blood cells are produced due to vitamin B12 deficiency. *TCN1* encodes the protein  
205 haptocorrin (also known as Transcobalamin-1) which binds vitamin B12 and is involved in its  
206 uptake <sup>29</sup>. Also, splice region variant rs1893592 causes increased expression of *UBASH3A* in  
207 most GTEx tissues, including thyroid. This signal colocalizes (H4>0.87) with self-reported  
208 treatment using the thyroid hormone sodium levothyroxine. Hypothyroidism is a common  
209 comorbidity with type 1 diabetes, for which there is strong evidence that *UBASH3A* is causal <sup>30</sup>.



210 Finally, the synonymous variant rs2228079 is the only credibly causal variant for an eQTL  
211 associated with altered *ADORA1* expression in whole blood (eQTLGen) and colocalizes with  
212 asthma in UK Biobank ( $H4 > 0.99$ ). *ADORA1* encodes a type of adenosine receptor, a class of  
213 proteins targeted by the approved drug (Theophylline) for the treatment of asthma.

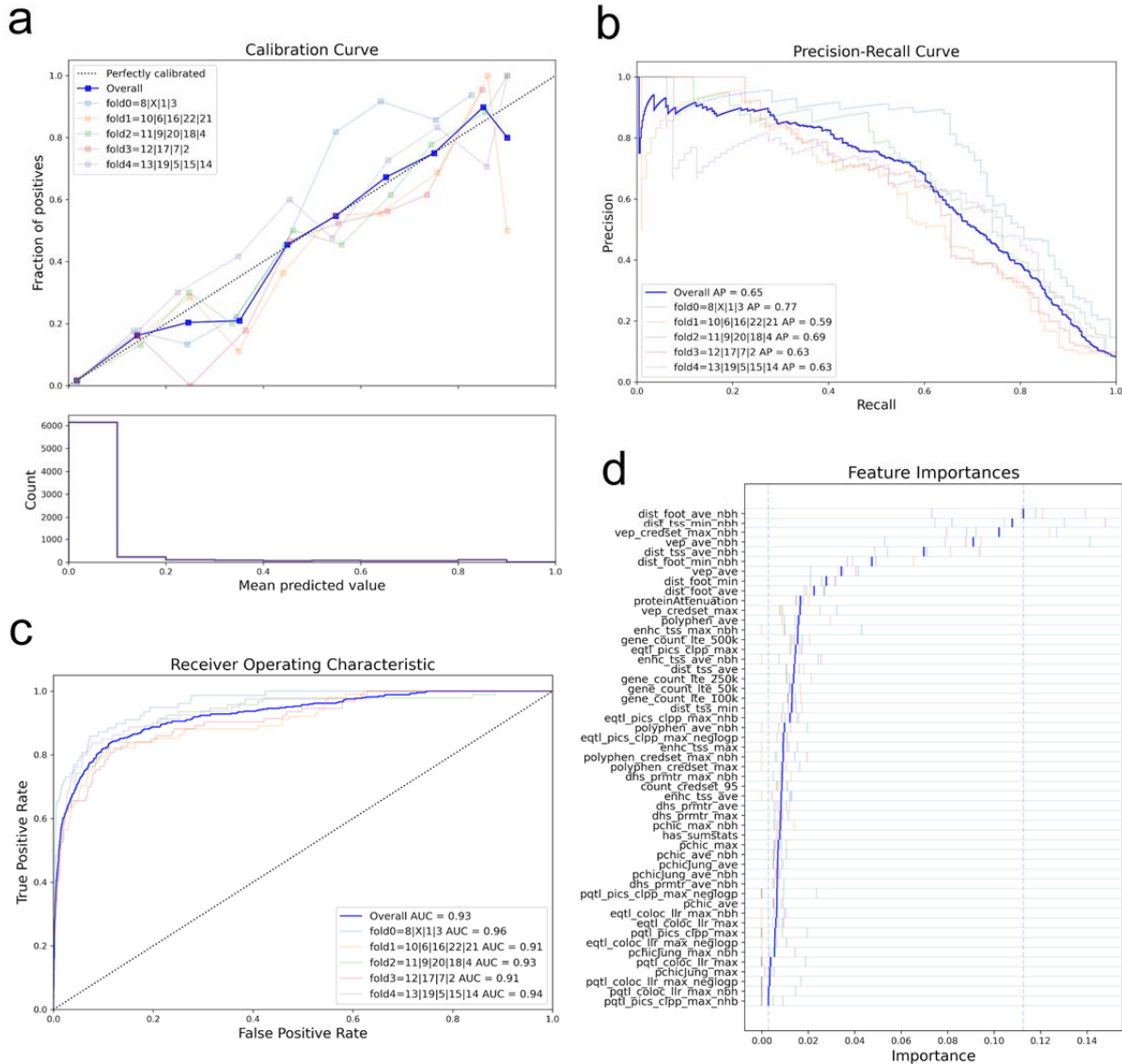
214  
215 Colocalization also provided strong genetic evidence for some less well known gene-disease  
216 associations (Supplementary Table 7). One example is splice region variant rs11589479, which  
217 causes increase in *ADAM15* expression in several monocytes states and also colocalizes  
218 ( $H4 = 0.99$ ) with Crohn's disease<sup>31</sup>. *ADAM15*, a disintegrin and metalloproteinase, is strongly  
219 upregulated in colon tissues from inflammatory bowel disease patients compared to healthy  
220 controls and plays a role in leukocyte trans-migration across epithelial and endothelial barriers  
221 as well as the differentiation of regenerative colonic mucosa<sup>32</sup>.

## 222 A machine learning model prioritizes genes at gold-standard loci

223 We next developed a "locus to gene" model (L2G) to prioritize causal protein-coding genes at  
224 GWAS loci by integrating our catalog of fine mapping associations with relevant functional  
225 genomics features. We first manually curated a set of 445 gold standard positive (GSP) genes  
226 at GWAS loci for which we are confident of the causal gene assignment (Supplementary Table  
227 8, see methods). The selected genes are based on (i) expert domain knowledge of strong  
228 orthogonal evidence or biological plausibility; (ii) known drug target-disease pairs; (iii)  
229 experimental alteration from literature reports (e.g. nucleotide editing); (iv) observational  
230 functional data (e.g. colocalizing molecular QTLs, colocalizing epigenetics marks, reporter  
231 assays) (Supplementary Table 9). Next, we defined locus-level predictive features from four  
232 evidence categories: in silico pathogenicity prediction from VEP and PolyPhen, colocalization of  
233 molecular QTLs, gene distance to credible set variants weighted by their fine-mapping  
234 probabilities, and chromatin interaction (Supplementary Table 10). The chromatin interaction  
235 data comprised promoter-capture Hi-C from 27 cell types<sup>33</sup>, FANTOM enhancer-TSS pairwise  
236 cap analysis of gene expression correlation<sup>34</sup>; and DNase I hypersensitive site-gene promoter  
237 correlation<sup>35</sup>. Then, using a nested cross-validation strategy, we trained a gradient boosting  
238 model to distinguish GSP genes from other genes within 500 kb at the same loci (see methods).

239  
240 The L2G model produced a well calibrated score, ranging from 0 to 1, which reflects the  
241 approximate fraction of GSP genes among all genes above a given threshold (Figure 2). At a

242 classification threshold of  $\geq 0.5$ , the full model correctly identified 238 out of 445 true positives  
243 with 86 false positives (average precision = 0.65; Table 1). We compared the full model against  
244 a naive nearest gene classifier (closest gene footprint and closest TSS), which selects the  
245 closest gene to each lead variant, and thus does not make use of other candidate variants from  
246 fine-mapping. The naive nearest gene classifier identified more true positives at the same  
247 threshold (268 out of 445) but at the cost of identifying 2.4 times more false positives (207)  
248 (Average precision=0.37). Hence the full L2G model has higher precision with a small reduction  
249 in recall.  
250



251

252 **Figure 2:** Performance of the locus-to-gene (L2G) model. (a) Calibration curve, showing (top)  
 253 the fraction of all GSP genes found as positives at different L2G score thresholds (mean  
 254 predicted value), and (bottom) the count of genes in each L2G score bin. (b) The precision-  
 255 recall curve and (c) the receiver-operator characteristic curve for identifying GSP genes from  
 256 among those within 500 kb at each locus. (d) The *Relative Importance* of each predictor in the  
 257 L2G model.

258

259 To identify which features are most important in predicting GSP genes, we retrained the model  
260 to include features from only one of the four evidence categories at a time (leave-one-group-in  
261 analysis). No individual feature set gets a higher ‘Average Prediction’ score as the full model  
262 (Table 1). Our ‘mean distance’ feature which aggregates across all the variants in the credible  
263 set and weighs by their posterior probability was the most predictive (average precision=0.62)  
264 followed by *in silico* pathogenicity prediction evidence (average precision=0.48), molecular QTL  
265 colocalization (average precision=0.36) and chromatin interaction (average precision=0.26)  
266 (Table 1, Leave-one-group-in section). Note that the ‘mean distance’ feature is distinct from a  
267 ‘naive closest gene distance’ feature because of the weighting across a credible set to the most  
268 likely SNPs, and thus manages to discard many false positives ( $FP_{mean\ distance} = 98$  vs  $FP_{naive}$   
269  $closest\ footprint\ gene} = 207$  and  $FP_{naive\ closest\ TSS\ gene} = 195$ ). Within the mean distance features  
270 tested, whether the gene was the closest at the locus using a gene footprint distance metric  
271 averaged over the credible set and whether the gene was the closest at the locus using the  
272 minimum gene-TSS distance over the 95% credible set, had the highest relative feature  
273 importances (Figure 2d). Thus, when using distance as a predictor of causal genes, the  
274 distance relative to other genes is more important than the absolute distance.  
275

Features	Average precision	AUC	Precision	Recall	TP	FP	TN	FN	Sensitivity	Specificity	FDR	GSP count	GSN count
Full model	0.65	0.93	0.73	0.53	236	86	6429	209	0.53	0.99	0.27	445	6515
<b>Naïve closest gene classification</b>													
Closest footprint	0.37	0.79	0.56	0.6	268	207	6308	177	0.6	0.97	0.44	445	6515
Closest TSS	0.34	0.76	0.56	0.55	246	195	6320	199	0.55	0.97	0.44	445	6515
<b>Leave-one-group-in</b>													
Mean Distance*	0.62	0.91	0.69	0.49	219	98	6417	226	0.49	0.98	0.31	445	6515
Interaction	0.26	0.79	0.55	0.05	23	19	6496	422	0.05	1	0.45	445	6515
Molecular QTL	0.36	0.85	0.62	0.18	79	49	6466	366	0.18	0.99	0.38	445	6515
Pathogenicity prediction	0.48	0.76	0.7	0.43	191	80	6435	254	0.43	0.99	0.3	445	6515
<b>Leave-one-group-out</b>													
Mean Distance*	0.47	0.77	0.69	0.43	191	84	6431	254	0.43	0.99	0.31	445	6515
Interaction	0.65	0.93	0.73	0.53	234	85	6430	211	0.53	0.99	0.27	445	6515
Molecular QTL	0.65	0.93	0.74	0.54	239	86	6429	206	0.54	0.99	0.26	445	6515
Pathogenicity prediction	0.63	0.92	0.71	0.5	222	91	6424	223	0.5	0.99	0.29	445	6515

276

277 **Table 1:** Classification performance for feature groups. Performance characteristics of the full  
 278 model are shown at the top, and analyses for individual groups of features are shown in  
 279 sections below. Counts are shown for true positives (TP), false positives (FP), true negatives  
 280 (TN), and false negatives (FN). \* Mean Distance aggregates across all the variants in the  
 281 credible set and weighs by their posterior probability.

282

283 We also assessed the unique contribution of each evidence type by leaving out one group of  
284 features at a time. Consistent with the leave-one-group-in analysis, dropping our mean distance  
285 features had the largest impact on prediction (*average precision* change from 0.65 to 0.47),  
286 followed by *in silico* pathogenicity prediction (*average precision* down to 0.63) (Table 1).  
287 Notably, when molecular QTL colocalization evidence was removed from the model we saw  
288 similar classification results, with 3 fewer true positives identified, and no net change in the Gold  
289 Standard Negatives (GSN)(Supplementary Table 11a). There are various possible reasons for  
290 this: the colocalization score may be redundant with some of our other features; we may lack the  
291 relevant tissue- or context-specific QTLs; or we may have obscured the utility of colocalization  
292 information by using a cross-tissue colocalization score. We also used a measure of *continuous*  
293 *reclassification improvement* to evaluate prediction changes across all possible classification  
294 thresholds. Here, adding molecular QTL colocalization evidence resulted in a net 4.7% GSPs  
295 having an increased prediction score and a net 42.2% GSNs having a decreased score  
296 (Supplementary Table 11b). This suggests that whilst our colocalization features do not provide  
297 sufficient evidence to support novel positives, lack of colocalization accurately identifies  
298 negative gene assignments. Removing chromatin interaction features resulted in a minor  
299 reduction in model performance (net 2 fewer GSPs) (Table 1).

300  
301 The low predictiveness of features apart from distance relates in part to their lower genome  
302 coverage. For distance features, most sentinel variants have at least 1 gene within 500 kb, but  
303 for pathogenicity, molecular QTL colocalization and chromatin interaction, coverage of variants  
304 was low (Supplementary Figure 2). Only a small proportion of studies had summary statistics  
305 available, limiting our ability to use *coloc* to perform a colocalization analysis (only 3% of all loci  
306 had *coloc* derived evidence). Our complimentary colocalization method, using a reference LD-  
307 panel to approximate summary statistics (the PICS method), increased the total number of loci  
308 with colocalization evidence to 19%. Evidence from pQTLs was very sparse at <1% coverage,  
309 which may account for its very low feature importance (Supplementary Figure 2).

## 310 Gene prioritization across all trait-associated loci

311 We used the trained L2G model to prioritize causal genes across all 133,441 trait-associated  
312 GWAS loci in our repository. At a classification threshold of 0.5, 55.4% (n=74,096) of all loci had  
313 a single gene prioritized whereas only 1.4% (n=1,907) had 2 or more genes prioritized  
314 (Supplementary Figure 3). 43.2% of loci did not reach the classification threshold. Across all

315 diseases, genes prioritized by the model were 7.8 times more likely (95% CI: [6.5, 9.3]) to be  
316 supported by literature evidence identified by text mining (Supplementary Table 12). Genes  
317 prioritized by the naive classifier using the closest gene footprint from the sentinel variant were  
318 also enriched (5.6 times, 95% CI: [4.7, 6.6]) but not as highly as the full model (p-value=0.008  
319 against null-hypothesis  $\log\text{OR}_{\text{Full model}} = \log\text{OR}_{\text{Naive model}}$ , Welch t-test).

320  
321 In order to benchmark the L2G versus the distance based classifier, we tested whether  
322 prioritized gene-diseases were enriched for known drug target-indication pairs across different  
323 clinical phases according to the ChEMBL database. Genes prioritized by the model were  
324 enriched with OR 7.4, 8.5 and 8.1 (95% CI: [5.7, 9.4], [6.3, 11.3], [5.7, 11.5]) across clinical trial  
325 phases  $\geq 2$ ,  $\geq 3$  and 4, respectively (Supplementary Table 13). Using a naive classifier we saw  
326 lower odds ratio point estimates but with overlapping confidence intervals (OR 5.3 [4.2, 6.7], 6.4  
327 [4.8, 8.5] and 6.7 [4.8, 9.3]) (Supplementary Figure 4). Thus the prioritisation using the L2G  
328 model both recapitulates the established enrichment of GWAS loci for known drugs<sup>11</sup> but also  
329 demonstrates that fine-mapping and colocalization combined with the L2G approach improves  
330 on their approach, and hence is likely to also improve success in identifying novel drug targets.

## 331 Discussion

332 To address the challenges of translating GWAS signals to biological insights, we developed a  
333 pipeline to format, harmonize, and aggregate human trait and disease GWAS, molecular QTLs  
334 and functional genomics data in a consistent way, providing statistical evidence for target  
335 prioritization across the entirety of GWAS traits and diseases. We then trained a machine  
336 learning model that integrates fine-mapping and functional genomics data to prioritize likely  
337 causal variants and genes at 133,441 trait-lead variant disease associations. The L2G score  
338 output by the model represents the likelihood that a gene is causal for that trait, subject to the  
339 limitations of our gold standard positive training data, and thus allows genes at all trait-  
340 associated loci to be ranked by the relative strength of their evidence. Under cross-validation,  
341 the model resulted in a 58% reduction in the number of false-positives detected (improved  
342 precision), at the cost of missing 11% of the gold-standard positives (reduction in recall). The  
343 top genes prioritized by the L2G score recover known relationships, including disease-gene

344 pairs with approved drugs, as well as novel disease-drug target associations that suggest  
345 potential novel therapeutic targets to pursue.

346

347 The strength of our machine learning approach stems from the systematic application of fine-  
348 mapping to obtain per-variant probabilities prior to gene assignment. Sentinel variants  
349 discovered by GWAS may not be the causal variant<sup>36</sup>; by aggregating functional data across  
350 the credible set we incorporate information from all plausible causal variants at the locus. Using  
351 a supervised learning method allowed us to efficiently combine heterogeneous functional  
352 datasets into a single model. The L2G score output by our model is well calibrated, meaning  
353 that it can be interpreted as a probability and thus the evidence supporting a gene assignment  
354 can be compared both within and between loci.

355

356 A limitation of our approach is that it requires a large number of high-quality gold standards to  
357 train the model, and each source of gold standards will have biases. For example, when we  
358 compared the dataset of drug targets from ChEMBL retrospectively mapped to GWAS loci to  
359 the manually curated datasets (mainly focused on the closest genes and those with known  
360 missense variants), we found that distance and VEP features performed much better in the  
361 manually curated datasets (Supplementary Figure 5), emphasizing the need to curate less-  
362 biased datasets. Using varied sources may help mitigate some source-specific biases, but  
363 manually curated allele-gene pairs are intrinsically more likely to be close to each other. Future  
364 gold-standard training data should represent a range of possible molecular mechanisms. The  
365 reliance on large amounts of training data influenced the design of our model. To avoid  
366 stratifying gold-standards into smaller subgroups, we trained the model across all diseases at  
367 once and using functional data ascertained from different tissues/cell types aggregated into a  
368 single feature. This means that the model is not currently able to specifically leverage the  
369 tissues/cell types that are most relevant for a given disease.

370

371 The outputs of our analyses can be viewed in the Open Targets Genetics portal  
372 (<https://genetics.opentargets.org>), a user-friendly web interface that supports visualisation of  
373 fine-mapping and L2G scores for individual variants and genes across 133,441 trait-lead variant  
374 GWAS associations. The portal also offers other features including disease-disease and  
375 disease-molecular traits colocalization analyses across ~3,600 GWAS summary statistics and  
376 92 tissue and cell type-specific molecular QTL summary statistics to identify traits and diseases  
377 that share common genetic susceptibility mechanisms. The portal will regularly be updated with



378 new GWAS summary statistics both from Europeans and non-European ancestries as well as  
379 QTLs and functional genomic data from a wider range of tissues and cell types. Planned  
380 enhancements include displaying tissue- and cell type-specific enrichments for each included  
381 trait, using methods such as CHEERS<sup>37</sup> that leverage functional annotations. These  
382 enrichments will also be used to improve the L2G model by using functional genomics data from  
383 tissues that are most relevant to each disease and trait. Our repository of gold-standard gene  
384 assignments will be expanded as more evidence arises. In particular, we encourage scientists  
385 from the genetics community to contribute to this repository, since having diverse evidence  
386 sources can partially address the bias that comes with manually curated sets.

## 387 Methods

### 388 **Summary statistics based fine mapping**

389 We harmonised summary statistics to ensure alleles and effect directions were consistent  
390 across studies, and removed variants with low confidence estimates (minor allele count < 10).  
391 We identified independently associated loci for each study using Genome-wide Complex Trait  
392 Analysis Conditional and Joint Analysis (GCTA-COJO; v1.91.3)<sup>21</sup>. UK Biobank genotypes  
393 down-sampled to 10k individuals were used as a linkage-disequilibrium (LD) reference for  
394 conditional analysis<sup>38</sup>. We considered a locus to be independently associated if both marginal  
395 and conditional p-values were less than  $5e^{-8}$ . For each independent locus, we produced a set of  
396 summary statistics that are conditional on all other independent loci  $\pm 2$ Mb from the sentinel  
397 variant. Using the conditional set of summary statistics, we computed approximate Bayes  
398 factors<sup>39</sup> from the beta and standard error for each SNP, with a variance prior (W) of 0.15 for  
399 quantitative traits and 0.2 for binary traits, and determined variant posterior probabilities (PP)  
400 assuming a single causal variant as:  $PP = \text{SNP BF} / \text{sum}(\text{all SNP BFs})$  for all SNPs within a  
401  $\pm 500$ Kb window. We considered any variant with a PP > 0.1% as being in the credible set.

### 402 **Linkage-disequilibrium based fine mapping**

403 In addition to the above fine mapping analysis, we conducted a complementary LD based  
404 approach which allowed us to leverage information from studies that lack full summary statistics.  
405 For each independent locus, we identified all variants in LD with the sentinel variant ( $R^2 > 0.5$  in  
406  $\pm 500$ Kb window). LD was calculated in 1000 Genomes phase 3 data<sup>40</sup> by mapping the GWAS  
407 study ancestries to the closest super population<sup>41</sup>, taking a sample size weighted-mean of the  
408 Fisher Z-transformed correlations in the case of multi-ancestry studies. We then used the

409 Probabilistic Identification of Causal SNPs (PICS) method to estimate the PP that each variant  
410 is causal based on the LD structure at each locus<sup>23</sup>. As above, we kept all variants with PP >  
411 0.1%.

#### 412 **Colocalization analysis**

413 Molecular QTL summary statistics were acquired from the EBI eQTL Catalogue<sup>16</sup>, GTEx (v7)<sup>14</sup>,  
414 eQTLGen<sup>15</sup> and Sun et al. protein QTLs<sup>17</sup>. Summary statistics were restricted to be  $\pm 1$ Mb from  
415 the gene transcription start site (TSS). We pre-processed and fine mapped molecular QTL  
416 summary statistics using the same method described above for GWAS studies. However, we  
417 used less stringent criteria for the inclusion of QTL lead variants, requiring minor allele count  $\geq 5$   
418 and adjusted for multiple testing using a Bonferroni correction of  $p < 0.05 / \text{number of variants}$   
419 tested per gene.

420  
421 For GWAS studies with summary statistics, we performed a colocalization analysis if there was  
422 at least 1 variant overlapping between the GWAS and molecular trait 95% credible sets (prior  
423 evidence for colocalization). We conducted colocalization of summary statistics using the coloc  
424 package (v.3.2-1)<sup>27</sup> with default priors. Given that there is prior evidence for colocalization,  
425 these parameters will give conservative estimates. As with the fine mapping pipeline, we used  
426 summary statistics conditional on all other independent loci within  $\pm 2$ Mb and restricted the coloc  
427 analysis to a  $\pm 500$ Kb window around each sentinel variant. A minimum of 250 intersecting  
428 variants were required for analysis.

429 For GWAS studies without summary statistics, we performed an alternative colocalization  
430 analysis using the LD-based PICS fine mapping sets. Colocalization was approximated by  
431 taking variants that intersect at pairs of GWAS and molecular trait loci, and summing the  
432 product of the PPs.

#### 433 **Pre-processing of functional genomics data for L2G prioritization**

434 We used 4 main classes of evidence to prioritize genes: (i) variant pathogenicity in silico  
435 predictions; (ii) colocalization with molecular trait quantitative trait loci (QTL); (iii) chromatin  
436 conformation; (iv) linear genomic distance from variant to gene.

437 We used *in silico* pathogenicity predictions to estimate the effect of variants on gene transcripts  
438 and protein function. Firstly, we incorporated Variant Effect Predictor (VEP)<sup>24</sup> transcript

439 consequences. We mapped VEP's impact ratings of High, Moderate, Low to scores of 1.0, 0.66,  
440 0.3 (respectively), and included an additional four consequences (intronic, 5' UTR, 3' UTR,  
441 nonsense-mediated mRNA decay transcript variants) with a score of 0.1 as we expected them  
442 to have predictive value through their functional consequences on mRNA transcription,  
443 secondary structure and translation. For each variant-gene pair we took the maximum score  
444 across transcripts. In addition to VEP we included PolyPhen-2 pathogenicity scores  
445 representing the probability that a non-synonymous substitution is damaging <sup>42</sup>.

446  
447 Chromatin interaction data were from promoter-capture Hi-C, FANTOM enhancer-TSS  
448 correlation, and DNase-hypersensitivity enhancer-promoter correlation. Each of the data points  
449 in these datasets is represented as a pair of interacting genomic intervals and an association  
450 statistic. We retained interval pairs with one end encompassing an Ensembl gene Transcription  
451 Start Site (TSS)<sup>43</sup> and the other end containing any variant in Gnomad 2.1 <sup>44</sup>, resulting in  
452 variant-gene pairs with a dataset-specific association statistic.

453  
454 We included two genomic distance metrics as it has been shown that, despite notable contrary  
455 exceptions, linear distance is a good predictor of candidate causal genes <sup>45</sup>. First, the distance  
456 from each variant to all gene TSSs is included. Second, the distance from each variant to each  
457 gene's footprint, where the footprint is any position between the start and end positions of the  
458 gene. For both metrics the canonical transcript is used, as defined by Ensembl for protein-  
459 coding genes within a  $\pm 500\text{Kb}$  window around each variant.

#### 460 **Derivation of locus-to-gene prioritization features**

461 We next combined our fine mapping and functional genomics data to create features to prioritize  
462 candidate causal genes at each trait-associated locus (locus-to-gene scoring) (Supplementary  
463 Table 10).

464  
465 Except for molecular trait colocalization evidence, each functional genomics dataset is variant-  
466 centric, meaning they give variant-to-gene scores. We convert variant-centric scores into locus-  
467 to-gene scores by aggregating over credible variants identified through fine mapping. For  
468 GWAS studies with summary statistics available we used ABF credible sets, otherwise we used  
469 LD-based PICS credible sets. We implemented two complementary methods for aggregating  
470 over credible sets. Firstly, we took a weighted sum of scores across all variants identified by fine

471 mapping (PP > 0.01%) using PP of causality as weights (Equation 1). Secondly, we took the  
472 maximum score for any variant in the 95% credible set (Equation 2).

473

$$weightedScore_{(study,locus,gene,source,tissue)} = \sum_{v=i}^n (score_{(i,gene,source,tissue)} \cdot pp_{(study,locus,i)})$$

474 Equation 1

$$maxScore_{(study,locus,gene,source,tissue)} = \max(score_{(i,gene,source,tissue)})$$

475 Equation 2

476

477 Molecular trait colocalization evidence is a locus-centric score. We included both summary  
478 statistic derived *coloc* evidence (Equation 3) and LD-derived colocalization evidence as  
479 features. Each GWAS signal may have colocalization estimates from multiple independent  
480 molecular trait signals (each conditional on the others), we therefore took the maximum score  
481 across estimates. Given that evidence against colocalization ( $h_3$ ) cannot be directly estimated  
482 without full summary statistics, this term was dropped for the LD-derived colocalization feature  
483 (Equation 4).

484

$$colocSumstatsScore_{(study,locus,qtlttype,tissue,gene)} = \max \text{ across molQTL loci} (\log_2(\frac{h4}{h3}))$$

485 Equation 3

486

$$colocLdScore_{(study,locus,qtlttype,tissue,gene)} = \max \text{ across molQTL loci} (\log_2(h4))$$

487 Equation 4

488

489 For functional genomics datasets with measurements in multiple tissues (or cell types), we  
490 calculated the locus-level feature for each tissue separately and took the maximum across  
491 tissues (Equation 5).

492

$$feature_{(study,locus,gene)} = \max \text{ across tissues} (feature_{(study,locus,tissue,gene)})$$

493 Equation 5

494

495 We next wanted to provide the model with information about other genes at each locus (termed  
496 the *neighbourhood* feature). This allows the model to learn whether a given gene has, for

497 example, the highest colocalization score compared to others at the locus. To do this we divided  
498 each feature by the maximum score across genes at that locus (Equation 6).  
499

$$\mathit{neighbourhoodFeature}_{(study,locus,gene)} = \frac{\mathit{feature}_{(study,locus,gene)}}{\max \text{ across genes}(\mathit{feature}_{(study,locus,genes)})}$$

500 Equation 6

### 501 **Curation of a GWAS gold-standard training dataset**

502 We next assembled a repository of published GWAS loci  
503 (<https://github.com/opentargets/genetics-gold-standards>) for which we have high confidence  
504 that the gene mediating the association is known. Gold-standard evidence were grouped into 4  
505 classes: (i) *expert curated* loci with strong orthogonal evidence or biological plausibility; (ii) *drug*  
506 loci inferred from known drug target-disease pairs; (iii) loci inferred from *experimental* alteration  
507 (e.g. nucleotide editing); (iv) loci inferred from *observational* functional data (e.g. colocalizing  
508 molecular QTLs). We also assigned each gold-standard a confidence rating of *high*, *medium* or  
509 *low* depending on our assessment of the strength of supporting evidence.

510  
511 We started by compiling existing gold-standard examples from the literature. 227 curated  
512 metabolite QTLs were sourced from Stacey *et al*<sup>45</sup> and a further 136 loci were curated by Eric  
513 Fauman with strong biological plausibility (Supplementary Table 6). We then ascertained 57  
514 genes with “causal” or “strong” *observational* data from the Type 2 Diabetes Knowledge Portal  
515 Effector Genes table, this equates to genes with: a confirmed causal coding variant; or at least  
516 two of the following: (i) a likely causal coding variant, (ii) >1 piece of regulatory evidence, >1  
517 piece of perturbation evidence<sup>46</sup>. We added a further 48 disease-causal genes curated from the  
518 literature. These were mainly GWAS associated loci that were fine-mapped and colocalized with  
519 eQTL and epigenomic features in disease-relevant tissues in order to prioritize likely functional  
520 variants and their causal genes. These results were then functionally validated using  
521 experiments such as reporter assays and CRISPR/Cas9 genome editing.

522  
523 In addition to literature sourced loci, gold-standard evidence was generated based on known  
524 drug-target-indication associations curated in ChEMBL in clinical trial phase II, III or IV<sup>47</sup>. Drugs  
525 that bind a protein complex, rather than a single protein, were removed unless the binding  
526 subunit was known. The ChEMBL evidence was combined with the genetics features to identify  
527 loci with known drug targets. Gold-standards derived from phase II, III and IV drug targets were  
528 assigned a confidence of *low*, *medium* and *high*, respectively. Additionally, confidences were

529 adjusted to indicate the distance of the sentinel variant to the drug target, variant-gene  
530 distances of < 500, 250, 100Kb kb were assigned confidences *low*, *medium* and *high*,  
531 respectively.

532  
533 Duplications were removed from the Gold-standard positives (GSP) list so that GWAS allele-  
534 gene pairs never occurred more than once in the training data. The same gene could occur as a  
535 GSP more than once if the associated alleles were independent, i.e. if no variants overlapped  
536 between their credible sets (using all variants with PP > 0.1%). All non-GSP genes in the  
537 training data at the locus ( $\pm 500\text{kb}$ ) were set as gold-standard negatives (GSN). GSNs genes  
538 were subsequently removed if they had a stringDB score  $\geq 0.7$  with the GSP at the same locus,  
539 the aim being to remove alternative explanations for the association between trait-associated  
540 allele and gene. This resulted in a total of 229 GSNs being removed (out of a total of 9,171). A  
541 total of 445 GSP were included in the final training data.

#### 542 **Supervised learning of locus-to-gene features**

543 We used all GWAS loci with high or medium confidence gold-standard evidence (445 loci) to  
544 train an XGBoost gradient boosting classifier<sup>48</sup> using a binary logistic learning objective  
545 function. Nested cross-validation (CV) as implemented in scikit-learn was used to maintain  
546 independence of the training and test data and to tune hyperparameters. The outer CV  
547 consisted of 5 folds split by chromosomes so that each group contained an approximately equal  
548 number of GSPs. Within each fold, we used a random parameter search to train 1000 models,  
549 which were assessed using a *balanced accuracy* metric averaged over 5 randomly split inner  
550 folds.

551  
552 For each group of features included in the main model, we conducted sub-analyses whereby  
553 either only that feature group was included (leave-one-group-in), or everything except that  
554 feature group was included (leave-one-group-out). This allowed us to evaluate the relative  
555 performance of each feature group individually. Additionally, we output the *Relative Importance*  
556 of each feature as implemented in the XGBoost model<sup>49</sup>.

#### 557 **Model internal validation**

558 Our cross-validation approach produces separate models for each of the 5 outer folds. We  
559 evaluated the performance of each model against the remaining 20% of loci not used for

560 training. We used *average precision* and *area under the receiver operator curve (AUC)* metrics  
561 to assess the classification across the full range of prediction probabilities outputted by the  
562 model. We also assess the performance of the model after applying a hard threshold of  $>0.5$   
563 ( $>50\%$  confidence that the characteristics of the observed locus is consistent with being a gold-  
564 standard positive locus).

565  
566 We compared the relative performance of leave-one-group-in and leave-one-group-out models  
567 by calculating the *net reclassification improvement* (NRI) of loci compared to the full model<sup>50</sup>.  
568 NRI measures the number of GSP loci that move above the classification threshold ( $>0.5$ ),  
569 compared to GSN that move below, when the model is updated. We also calculate *continuous*  
570 *NRI (cNRI)*, the sum of the percentage of GSPs with classification scores that move in the  
571 correct direction vs. GSNs that move in the wrong direction (towards higher scores)<sup>51</sup>.

#### 572 **Model external validation with literature evidence**

573 We benchmarked the L2G assignment against independent gene-disease associations scored  
574 by literature mining in the Open Targets Platform. We excluded any publications for studies  
575 curated in GWAS Catalog to ensure independence of the training data. We restricted analyses  
576 to a subset of 22 prioritized diseases (Coronary artery disease, Breast carcinoma, Prostate  
577 carcinoma, Acute lymphoblastic leukemia, Inflammatory bowel disease, Crohn's disease,  
578 Ulcerative colitis, Rheumatoid arthritis, Osteoarthritis, Type I diabetes mellitus, Hypothyroidism,  
579 Psoriasis, Atopic eczema, Asthma, Alzheimer's disease, Parkinson's disease, Ankylosing  
580 spondylitis, Celiac disease, Gout, Multiple sclerosis, Systemic lupus erythematosus). For each  
581 disease, we constructed a 2x2 contingency table of 'gene prioritised by L2G model (score  $>$   
582  $0.5$ )' and 'gene prioritised by Open Targets literature evidence (top decile [ $>0.52$ ])'. Only genes  
583 scored by the L2G model ( $\pm 500$ kb of a sentinel GWAS variant) were included in the contingency  
584 table. We calculated enrichment and statistical significance using Fisher's exact test.

#### 585 **Enrichment of known drug targets**

586 We calculated drug target enrichment using known target-indication pairs curated in ChEMBL  
587 (accessed: 2019-03-25). We constructed a single 2x2 contingency table pooling across all  
588 indications, which consisted of 'gene prioritized by L2G model (score  $> 0.5$ )' and 'gene is known  
589 target of drug for indication matched to GWAS disease phenotype'. GWAS studies were only  
590 included if they could be mapped to a ChEMBL indication (matched using Experimental Factor  
591 Ontology) and that indication has a known drug that can be mapped to a protein-coding gene  
592 that was scored by the L2G model. Enrichment was calculated by Fisher's exact test.

## 593 Data availability

594 Our results are freely available through a web portal ([genetics.opentargets.org](https://genetics.opentargets.org)), GraphQL API  
595 or through bulk download. GWAS gold standard genes: [github.com/opentargets/genetics-gold-](https://github.com/opentargets/genetics-gold-standards)  
596 standards.

## 597 Acknowledgements

598 The authors would like to thank Ellen McDonagh, Joe Maranville, and David Hulcoop for their  
599 useful feedback to improve the paper and Helen Parkinson and Jackie MacArthur for their  
600 support with the GWAS Catalog data. This research has been conducted using the UK Biobank  
601 Resource. This work was funded by Open Targets. EM work was funded by JDRF (4-SRA-  
602 2017-473-A-N) to the Diabetes and Inflammation Laboratory, University of Oxford.

## 603 Author contributions

604 MG, JS, EM, ID wrote the manuscript. EM conducted the analysis and designed and built the  
605 ML model. EM, EMS, MG prioritised GWAS studies for curation by GWAS Catalog. EM, MC,  
606 AB, JH, EP curated and processed the GWAS and functional genomics data, EF, EM, MG  
607 curated the gold standards. GP, AM, LF, AH, EP designed and implemented visualisations for  
608 analysis. DO performed additional analysis. ID, MG, JAT, JCB conceived and supervised the  
609 study. MAK generated Figure 1. MG, EM, EMS, DW, EP worked on the biological questions and  
610 the underlying visualisations in the portal.

611

## 612 Competing interests

613 The authors do not have any conflicts of interest to declare.

## 614 References

- 615 1. Hindorff, L. A. *et al.* Potential etiologic and functional implications of genome-wide  
616 association loci for human diseases and traits. *Proc. Natl. Acad. Sci. U. S. A.* **106**, 9362–  
617 9367 (2009).
- 618 2. Altshuler, D., Daly, M. J. & Lander, E. S. Genetic mapping in human disease. *Science* **322**,  
619 881–888 (2008).
- 620 3. Claussnitzer, M. *et al.* FTO Obesity Variant Circuitry and Adipocyte Browning in Humans.  
621 *N. Engl. J. Med.* **373**, 895–907 (2015).



- 622 4. Zhu, Z. *et al.* Integration of summary data from GWAS and eQTL studies predicts complex  
623 trait gene targets. *Nat. Genet.* **48**, 481–487 (2016).
- 624 5. Brænne, I. *et al.* Prediction of Causal Candidate Genes in Coronary Artery Disease Loci.  
625 *Arterioscler. Thromb. Vasc. Biol.* **35**, 2207–2217 (2015).
- 626 6. Fachal, L. *et al.* Fine-mapping of 150 breast cancer risk regions identifies 191 likely target  
627 genes. *Nat. Genet.* **52**, 56–73 (2020).
- 628 7. Xue, A. *et al.* Genome-wide association analyses identify 143 risk variants and putative  
629 regulatory mechanisms for type 2 diabetes. *Nat. Commun.* **9**, 2941 (2018).
- 630 8. Okada, Y. *et al.* Genetics of rheumatoid arthritis contributes to biology and drug discovery.  
631 *Nature* **506**, 376–381 (2014).
- 632 9. Fang, H. *et al.* A genetics-led approach defines the drug target landscape of 30 immune-  
633 related traits. *Nat. Genet.* **51**, 1082–1091 (2019).
- 634 10. Hay, M., Thomas, D. W., Craighead, J. L., Economides, C. & Rosenthal, J. Clinical  
635 development success rates for investigational drugs. *Nat. Biotechnol.* **32**, 40–51 (2014).
- 636 11. Nelson, M. R. *et al.* The support of human genetic evidence for approved drug indications.  
637 *Nat. Genet.* **47**, 856–860 (2015).
- 638 12. Carvalho-Silva, D. *et al.* Open Targets Platform: new developments and updates two years  
639 on. *Nucleic Acids Res.* **47**, D1056–D1065 (2019).
- 640 13. Koscielny, G. *et al.* Open Targets: a platform for therapeutic target identification and  
641 validation. *Nucleic Acids Res.* **45**, D985–D994 (2017).
- 642 14. Consortium, G. & GTEx Consortium. Genetic effects on gene expression across human  
643 tissues. *Nature* vol. 550 204–213 (2017).
- 644 15. Võsa, U. *et al.* Unraveling the polygenic architecture of complex traits using blood eQTL  
645 metaanalysis. *bioRxiv* 447367 (2018) doi:10.1101/447367.
- 646 16. Kerimov, N. *et al.* eQTL Catalogue: a compendium of uniformly processed human gene  
647 expression and splicing QTLs. doi:10.1101/2020.01.29.924266.
- 648 17. Sun, B. B. *et al.* Genomic atlas of the human plasma proteome. *Nature* **558**, 73–79 (2018).
- 649 18. Buniello, A. *et al.* The NHGRI-EBI GWAS Catalog of published genome-wide association  
650 studies, targeted arrays and summary statistics 2019. *Nucleic Acids Res.* **47**, D1005–  
651 D1012 (2019).
- 652 19. Zhou, W. *et al.* Efficiently controlling for case-control imbalance and sample relatedness in  
653 large-scale genetic association studies. *Nat. Genet.* **50**, 1335–1341 (2018).
- 654 20. Lab, N. UK Biobank bulk summary statistics. <http://www.nealelab.is/uk-biobank>.
- 655 21. Yang, J. *et al.* Conditional and joint multiple-SNP analysis of GWAS summary statistics  
656 identifies additional variants influencing complex traits. *Nat. Genet.* **44**, 369–75, S1–3  
657 (2012).
- 658 22. Wellcome Trust Case Control Consortium *et al.* Bayesian refinement of association signals  
659 for 14 loci in 3 common diseases. *Nat. Genet.* **44**, 1294–1301 (2012).
- 660 23. Farh, K. K.-H. *et al.* Genetic and epigenetic fine mapping of causal autoimmune disease  
661 variants. *Nature* **518**, 337–343 (2015).
- 662 24. McLaren, W. *et al.* The Ensembl Variant Effect Predictor. *Genome Biol.* **17**, 122 (2016).
- 663 25. Michailidou, K. *et al.* Association analysis identifies 65 new breast cancer risk loci. *Nature*  
664 **551**, 92–94 (2017).
- 665 26. Kawase, T. *et al.* PH domain-only protein PHLDA3 is a p53-regulated repressor of Akt. *Cell*  
666 **136**, 535–550 (2009).
- 667 27. Giambartolomei, C. *et al.* Bayesian test for colocalisation between pairs of genetic  
668 association studies using summary statistics. *PLoS Genet.* **10**, e1004383 (2014).
- 669 28. Burgess, S. *et al.* Guidelines for performing Mendelian randomization investigations.  
670 *Wellcome Open Research* vol. 4 186 (2019).
- 671 29. Surendran, S. *et al.* An update on vitamin B12-related gene polymorphisms and B12 status.  
672 *Genes Nutr.* **13**, 2 (2018).

- 673 30. Todd, J. A. Evidence that UBASH3 is a causal gene for type 1 diabetes. *European journal*  
674 *of human genetics: EJHG* vol. 26 925–927 (2018).
- 675 31. de Lange, K. M. *et al.* Genome-wide association study implicates immune activation of  
676 multiple integrin genes in inflammatory bowel disease. *Nat. Genet.* **49**, 256–261 (2017).
- 677 32. Mosnier, J.-F. *et al.* ADAM15 upregulation and interaction with multiple binding partners in  
678 inflammatory bowel disease. *Lab. Invest.* **86**, 1064–1073 (2006).
- 679 33. Jung, I. *et al.* A compendium of promoter-centered long-range chromatin interactions in the  
680 human genome. *Nat. Genet.* **51**, 1442–1449 (2019).
- 681 34. Andersson, R. *et al.* An atlas of active enhancers across human cell types and tissues.  
682 *Nature* **507**, 455–461 (2014).
- 683 35. Thurman, R. E. *et al.* The accessible chromatin landscape of the human genome. *Nature*  
684 **489**, 75–82 (2012).
- 685 36. Visscher, P. M., Brown, M. A., McCarthy, M. I. & Yang, J. Five years of GWAS discovery.  
686 *Am. J. Hum. Genet.* **90**, 7–24 (2012).
- 687 37. Soskic, B. *et al.* Chromatin activity at GWAS loci identifies T cell states driving complex  
688 immune diseases. *Nat. Genet.* **51**, 1486–1493 (2019).
- 689 38. Bycroft, C. *et al.* The UK Biobank resource with deep phenotyping and genomic data.  
690 *Nature* **562**, 203–209 (2018).
- 691 39. Wakefield, J. Bayes factors for genome-wide association studies: comparison with P-  
692 values. *Genet. Epidemiol.* **33**, 79–86 (2009).
- 693 40. Consortium, T. 1000 G. P. & The 1000 Genomes Project Consortium. A global reference  
694 for human genetic variation. *Nature* vol. 526 68–74 (2015).
- 695 41. Morales, J. *et al.* A standardized framework for representation of ancestry data in genomics  
696 studies, with application to the NHGRI-EBI GWAS Catalog. *Genome Biol.* **19**, 21 (2018).
- 697 42. Adzhubei, I. A. *et al.* A method and server for predicting damaging missense mutations.  
698 *Nat. Methods* **7**, 248–249 (2010).
- 699 43. Zerbino, D. R. *et al.* Ensembl 2018. *Nucleic Acids Res.* **46**, D754–D761 (2018).
- 700 44. Karczewski, K. J. *et al.* The mutational constraint spectrum quantified from variation in  
701 141,456 humans. *Nature* **581**, 434–443 (2020).
- 702 45. Stacey, D. *et al.* ProGeM: a framework for the prioritization of candidate causal genes at  
703 molecular quantitative trait loci. *Nucleic Acids Res.* **47**, e3 (2019).
- 704 46. Type 2 Diabetes Knowledge Portal.  
705 <http://www.type2diabetesgenetics.org/gene/effectorGeneTable> (2019).
- 706 47. Gaulton, A. *et al.* The ChEMBL database in 2017. *Nucleic Acids Res.* **45**, D945–D954  
707 (2017).
- 708 48. Chen, T. & Guestrin, C. XGBoost. *Proceedings of the 22nd ACM SIGKDD International*  
709 *Conference on Knowledge Discovery and Data Mining - KDD '16* (2016)  
710 doi:10.1145/2939672.2939785.
- 711 49. Friedman, J. H. Greedy function approximation: A gradient boosting machine. *Ann. Stat.*  
712 **29**, 1189–1232 (2001).
- 713 50. Pencina, M. J., D'Agostino, R. B., D'Agostino, R. B. & Vasan, R. S. Evaluating the added  
714 predictive ability of a new marker: From area under the ROC curve to reclassification and  
715 beyond. *Statistics in Medicine* vol. 27 157–172 (2008).
- 716 51. Pencina, M. J., D'Agostino, R. B., Sr & Steyerberg, E. W. Extensions of net reclassification  
717 improvement calculations to measure usefulness of new biomarkers. *Stat. Med.* **30**, 11–21  
718 (2011).

720

721

722